Suppression of Dwarf and *irregular xylem* Phenotypes Generates Low-Acetylated Biomass Lines in Arabidopsis[1][OPEN]

Matthieu Bensussan, Valérie Lefebvre[2], Aloïse Ducamp, Jacques Trouverie[3], Emilie Gineau, Marie-Noëlle Fortabat, Alexia Guillebaux, Aurélie Baldy, Delphine Naquin, Stéphane Herbette, Catherine Lapierre, Gregory Mouille, Christine Horlow, and Mylène Durand-Tardif*

Institut National de la Recherche Agronomique, Institut Jean-Pierre Bourgin, Unité Mixte de Recherche 1318, Equipe de Recherche Labellisée Centre National de la Recherche Scientifique 3559, Saclay Plant Sciences, F–78026 Versailles, France (M.B., V.L., A.D., J.T., E.G., M.-N.F., A.G., A.B., C.L., G.M., C.H., M.D.-T.); Centre de Génétique Moléculaire, Unité Propre de Recherche 3404, Centre National de la Recherche Scientifique, Fédération de Recherche Centre National de la Recherche Scientifique 3115, F–91198 Gif-sur-Yvette, France (D.N.); and Clermont Université, Université Blaise Pascal, and Institut National de la Recherche Agronomique, Unité Mixte de Recherche 547 Physique et Physiologie Intégratives de l'Arbre Fruitier et Forestier, F–63000 Clermont-Ferrand, France (S.H.)

ORCID IDs: 0000-0002-1771-8049 (M.B.); 0000-0003-4843-0934 (E.G.); 0000-0002-1226-6071 (S.H.).

eskimo1-5 (*esk1-5*) is a dwarf Arabidopsis (*Arabidopsis thaliana*) mutant that has a constitutive drought syndrome and collapsed xylem vessels, along with low acetylation levels in xylan and mannan. ESK1 has xylan *O*-acetyltransferase activity in vitro. We used a suppressor strategy on *esk1-5* to screen for variants with wild-type growth and low acetylation levels, a favorable combination for ethanol production. We found a recessive mutation in the *KAKTUS* (*KAK*) gene that suppressed dwarfism and the collapsed xylem character, the cause of decreased hydraulic conductivity in the *esk1-5* mutant. Backcrosses between *esk1-5* and two independent knockout *kak* mutants confirmed suppression of the *esk1-5* effect. *kak* single mutants showed larger stem diameters than the wild type. The *KAK* promoter fused with a reporter gene showed activity in the vascular cambium, phloem, and primary xylem in the stem and hypocotyl. However, suppression of the collapsed xylem phenotype in *esk1 kak* double mutants was not associated with the recovery of cell wall *O*-acetylation or any major cell wall modifications. Therefore, our results indicate that, in addition to its described activity as a repressor of endoreduplication, KAK may play a role in vascular development. Furthermore, orthologous *esk1 kak* double mutants may hold promise for ethanol production in crop plants.

[1] This work was supported by Gautier Semences (to M.B.), by the Agence Nationale pour la Recherche (grant no. GPLA07–004 to V.L. and J.T.), and by the Bioénergies, Biomolécules et Matériaux Biosourcés du Carbone Renouvelable program Hemicoat (to E.G.).

[2] Present address: Laboratoire Biologie des Plantes et Innovation, EA 3900, Unité de Formation et de Recherche des Sciences, Université de Picardie Jules Verne, 80039 Amiens, France.

[3] Present address: Ecophysiologie Végétale, Agronomie, et Nutritions Azote, Carbone, Soufre, Unité Mixte de Recherche Institut National de la Recherche Agronomique 950, Université de Caen Basse-Normandie, 14032 Caen, France.

* Address correspondence to mylene.durand-tardif@versailles.inra.fr.

The author responsible for distribution of materials integral to the findings presented in this article in accordance with the policy described in the Instructions for Authors (www.plantphysiol.org) is: Mylène Durand-Tardif (mylene.durand-tardif@versailles.inra.fr).

M.B. designed and conducted most of the experiments and wrote the first draft of the article; V.L., A.D., J.T., and M.-N.F., performed the EMS mutagenesis, screened for suppressed phenotypes, and carried out the genetics for *BEEM396b* identification; A.G., A.B., and C.H. participated in the cytology and gene expression experiments; D.N. set up the pipeline to process the NGS data; C.L., E.G., and G.M. directed and performed the chemical analysis; S.H. performed and interpreted the conductivity measurements; M.D.-T. led the program, obtained the funding, and coordinated and compiled authors' contributions to the final version of the article; all the authors participated in the analysis of data and interpretation of results.

[OPEN] Articles can be viewed without a subscription.

www.plantphysiol.org/cgi/doi/10.1104/pp.15.00122

Today, the fields of agriculture and forestry must address challenging issues, particularly in the context of fluctuating environmental conditions, such as ensuring that food and feed production remain efficient, meeting societal demands to reduce inputs, including water, and creating new products, such as biofuel. The demand for biofuel, a renewable alternative to fossil fuel, further increases the need to develop biomass amenable to alcohol fermentation. Second-generation biofuels are based on the fermentation of sugars extracted from lignocellulosic biomass, which is produced from the residues of food crops or from nonfood crops; therefore, its production does not compete with food crops (Sims et al., 2010). This lignocellulosic biomass is made up of secondary cell walls, mostly found in vascular tissues.

Vascular tissues consist of a network of conduits, spanning an entire plant and connecting biosynthetically active leaves to the soil via the root and the shoot. There are two main vascular tissues, the xylem and the phloem, which arise from a lateral meristem called the procambium during primary growth. When dicot plants undergo secondary growth and cell walls are thickening, a secondary meristem, called the cambium or vascular cambium, emerges, giving rise to secondary vascular tissues (Esau, 1965; Buvat, 1989). The xylem is responsible for the upward transport of water and nutrients

from the soil to the whole plant. The phloem, positioned parallel to the xylem, supplies sink organs (roots, etc.) with leaf photoassimilates. In angiosperms, such as Arabidopsis (*Arabidopsis thaliana*), the xylem is composed of two main cellular types, tracheary elements, involved in the transport of water, and fibers, playing a major role in plant support (Turner and Sieburth, 2003). The function of the xylem depends on the plant's capacity to form thick secondary cell walls that confer mechanical strength to resist gravity and withstand negative pressure, allowing sap to travel upward through vessels. Xylem tissue is a major carbon sink that incorporates sugars into biopolymers (Ragni et al., 2011). Xylem secondary cell walls are mainly composed of cellulose embedded in a matrix of lignin and hemicelluloses. Xylan is a major hemicellulose in monocot and dicot secondary cell walls (Faik, 2010). Xylan has a linear backbone of β-(1,4)-linked D-Xyl residues that can be mono- or di-*O*-acetylated at positions O-2 and O-3 of the xylosyl residues (Ebringerova and Heinze, 2000).

O-Acetylation of polysaccharides reportedly has a negative effect on the utilization of lignocellulose, such as in the production of paper and bioethanol (Biely, 1985; Grohmann et al., 1989). A major xylan acetyltransferase was recently identified in Arabidopsis: TRICHOME BIREFRINGENCE-LIKE29/ESKIMO1 (TBL29/ESK1; Urbanowicz et al., 2014). *esk1* knockout mutants show a 60% reduction in xylan acetylation and a lesser reduction in mannan acetylation (Xiong et al., 2013; Yuan et al., 2013). *esk1* has been described previously as a genotype with drought stress symptoms (Bouchabke-Coussa et al., 2008; Lugan et al., 2009); its collapsed xylem vessels (*irregular xylem* [*irx*] phenotype) are assumed to be the cause of the drastic hydraulic conductivity drop, and thus the drought stress syndrome, including dwarfism (Lefebvre et al., 2011).

To identify new mutations that restore plant stature but maintain a low xylan *O*-acetylation level, we explored the possibility of producing this combination by screening an *esk1-5* ethyl methanesulfonate (EMS)-mutagenized population for nondwarf phenotypes. The suppressors of *esk1* were called *beem*, for biomass enhancement in *esk1-5* mutation background. Here, we describe the identification of one *BEEM* gene as *KAKTUS/UBIQUITIN PROTEIN LIGASE3* (*KAK/UPL3*), which encodes a protein belonging to the E3-ubiquitin protein ligase family (Downes et al., 2003).

RESULTS

esk1-5 Dwarfism Is Partially Suppressed by *kak* Mutations

Seeds produced by the *esk1-5/tbl29-1* mutant underwent EMS-induced mutagenesis. The resulting M2 population was screened for enhanced rosette size compared with *esk1-5*. Twelve independent M2 lines with a rosette size intermediate to *esk1-5* and the wild type were isolated and named *beem*. This work will focus on one of these lines, called *beem396b* (Fig. 1). A mapping-by-sequencing strategy, similar to methods described recently (Abe et al., 2012; Hartwig et al., 2012), was used to identify the causative mutation. The *beem396b* M2 line was backcrossed twice to its mutant background *esk1-5*. The resulting F2 population showed a 124:446 segregation (χ^2 test for an expected segregation of 1:3; $P = 0.0735$) for rosette size, suggesting that a single recessive mutation was responsible for the suppressed phenotype. DNA from the 124 plants exhibiting the enlarged rosette phenotype compared with *esk1-5* was extracted, pooled in equimolar ratios, and sequenced using Illumina whole-genome sequencing (Supplemental Protocol S1). Predicted variants were ranked by their likelihood of being the causative mutation (Supplemental Protocol S2). The mutation index was mapped along chromosomes and peaked at a unique locus at the bottom of chromosome 4 (base 18045924; The Arabidopsis Information Resource 10 [TAIR10] genome release) with a frequency of 84% (Supplemental Fig. S1; Abe et al., 2012). We attribute the less-than-perfect peak frequency (less than 100%) to the selection of false-positive F2 plants. The mutation with the highest index was a 1-bp deletion causing a frame shift within the *KAK/UPL3* (AT4G38600) gene coding sequence. The deletion causes an Ala-to-Val amino acid change at codon 861 of the *KAK* coding sequence and a premature stop codon six nucleotides after the deletion at codon 863, likely leading to the translation of a truncated KAK protein (Fig. 2; Supplemental Fig. S2).

KAK has been described as a repressor of endoreduplication in trichomes, with *kak* mutants exhibiting overbranched trichomes associated with high nuclear DNA content (Perazza et al., 1999; El Refy et al., 2003). In this work, the leaves of *kak* mutants harbored over 80% of trichomes having four or five branches, while the wild type exhibited mainly three-branched trichomes and a minority of two- and four-branched trichomes (Supplemental Fig. S3). The observation of overbranched trichomes has been correlated with a transfer DNA (T-DNA) insertion in the *KAK* gene (Perazza et al., 1999; El Refy et al., 2003). Observation of leaf trichomes using scanning electron microscopy showed that *beem396b* had a typical *kak* mutant phenotype, whereas the starting *esk1-5* mutant had normal trichomes (Supplemental Fig. S3). Among the independent *beem* lines isolated, only *beem308a* also presented an overbranched trichome phenotype (Supplemental Fig. S4). Large rosettes and trichome overbranching were observed in F1 plants from a cross between *beem396b* and *beem308a*, suggesting that the lines are allelic. Sequencing PCR products (primers are listed in Supplemental Table S1) of the full *KAK* genomic sequence in *beem308a* identified a C-to-T transition (position 18043667; TAIR10) within the *KAK* coding sequence, causing a premature stop codon at codon 1,469 of the KAK protein, likely leading to the translation of a truncated KAK protein (Supplemental Fig. S4). The isolation of the *beem308a* line in our screen for suppressor lines provided further support to our supposition that *KAK* inactivation suppresses *esk1* dwarfism. Nevertheless, *beem308a* was not studied further due to the presence of an additional early-flowering mutation that impaired morphometric comparisons between genotypes.

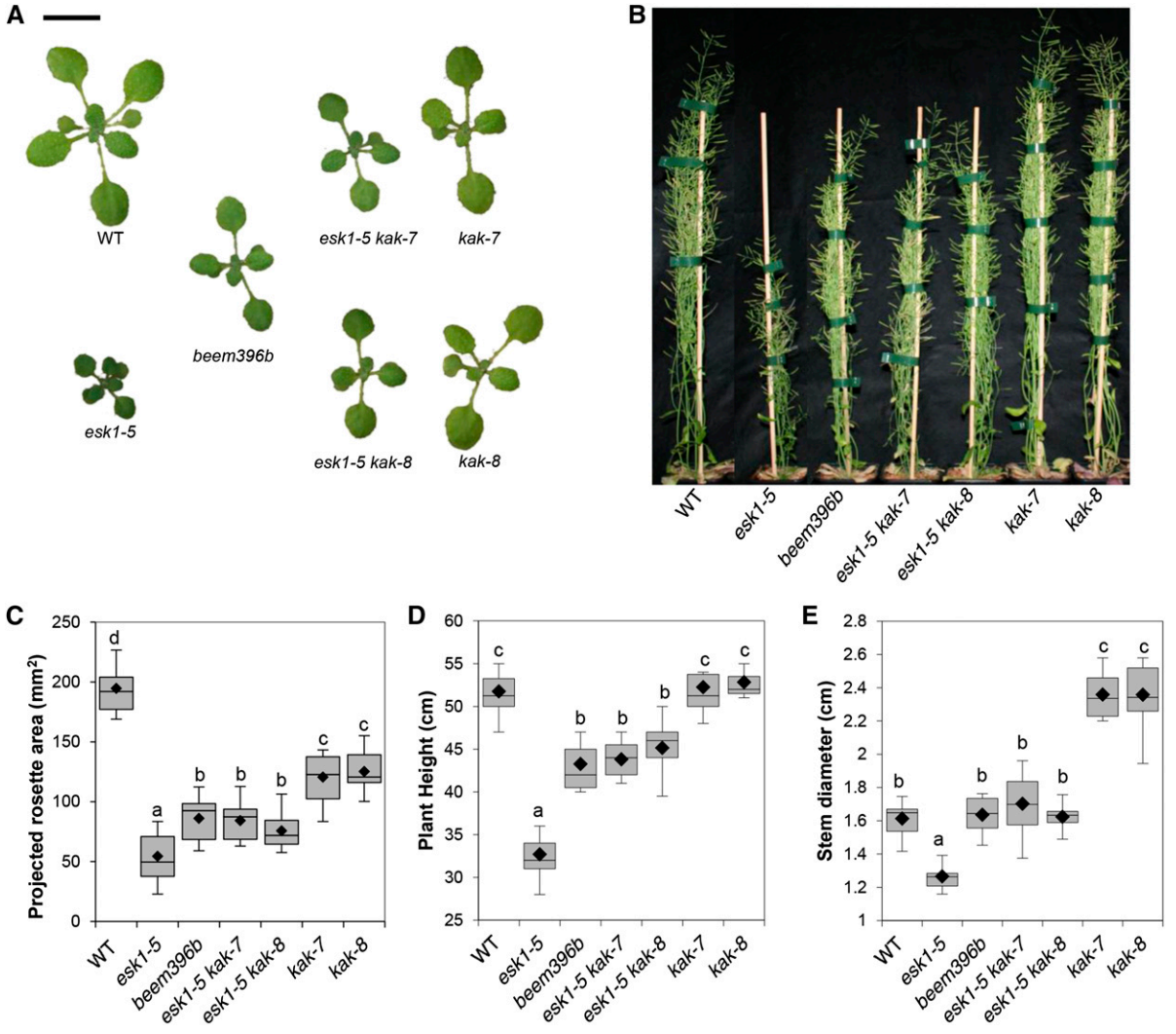

Figure 1. Partial suppression of *esk1-5* dwarfism by *kak* mutations. A, Rosettes of 2-week-old plants. Bar = 1 cm. B, Twelve-week-old mature plants. Bar = 5 cm. C, Rosette area of 2-week-old plants. D, Length of the main inflorescence stem of mature 12-week-old plants. E, Diameter of the main inflorescence stem of mature 12-week-old plants. WT, Wild type. In C to E, the box and whisker plots show the distribution of 12, eight, and eight measurements, respectively. Black diamonds represent the means, lines represent medians, top and bottom ends of the boxes represent the first and third quartiles, respectively, and whisker extremities represent maximum and minimum data points. Letters above the boxes indicate groups with significant differences as determined by Tukey's multiple pairwise comparisons test.

To confirm that *KAK* inactivation suppresses *esk1* dwarfism, we generated and studied *esk1-5 kak* double mutants with two independent T-DNA insertion lines within the *KAK* gene (Fig. 2). *kak-7* and *kak-8* exhibited the typical overbranched trichome phenotype (Supplemental Fig. S3). The rosette surface areas of 2-week-old *kak-7* and *kak-8* plants were significantly smaller than that of the wild type (Fig. 1), but mature rosette area at bolting (M. Durand-Tardif, unpublished data) and stem height were not significantly different from the wild type (Fig. 1). The stem diameter of *kak-7* and *kak-8* was significantly larger than in the wild type (Fig. 1). Two double mutants, *esk1-5 kak-7* and *esk1-5 kak-8*, both showed typical *kak* mutant trichomes (Supplemental Fig. S3) and an enlarged rosette size, as observed in *beem396b* (Fig. 1). Morphometric parameters, such as rosette area of 2-week-old plantlets and mature rosette size at bolting (M. Durand-Tardif, unpublished data), stem height, and stem diameter (Fig. 1), showed that *esk1-5 kak* double mutants perform better than *esk1-5* but show values similar to those in the *beem* lines. These data confirm the involvement of *kak* mutations in the increase in rosette size observed in the *esk1-5* mutant. Moreover, *kak* inactivation did not affect *ESK1* transcription, as shown in Supplemental Figure S5; as described elsewhere, the *ESK1* transcript is expressed in stems of the wild type and in both *kak* single mutants (Xin and Browse, 1998). No *ESK1* transcript was observed in genotypes carrying the *esk1-5* mutation. However, *esk1-5 kak* double mutants showed significantly smaller rosette areas than the *kak* single mutants. As

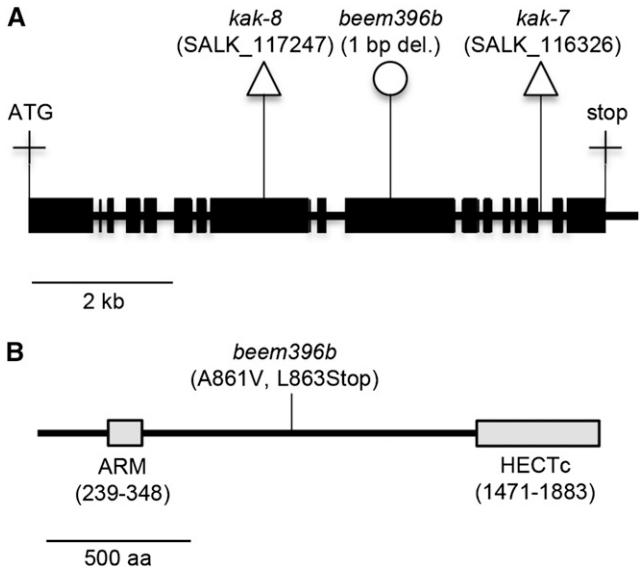

Figure 2. EMS mutation in *beem396b* generates a stop codon in the *KAK* gene. A, *KAK* gene model. Exons are represented by black boxes, and introns and the noncoding 3′ region are represented by the black line. Triangles indicate T-DNA insertions, and the circle indicates the EMS-induced mutation. B, Position of the EMS-induced mutation within the KAK protein sequence. Gray boxes represent conserved domains: ARM, Armadillo/β-catenin-like repeats motif responsible for the specific interaction of *KAK* with proteins targeted for degradation; HECTc, catalytic domain responsible for the transfer of polyubiquitin chains from ubiquitin-conjugating enzymes (E2) to proteins targeted for degradation. aa, Amino acids.

expected, the suppression of dwarfism in *beem396b* is not due to the restoration of *ESK1* expression.

The Suppression of Dwarfism Is Not Associated with the Recovery of Cell Wall Acetylation or Major Cell Wall Modifications

The collapsed xylem phenotype in the *esk1-5* mutant is primarily caused by a strong reduction in xylan, and possibly mannan, *O*-acetylation (Xiong et al., 2013; Yuan et al., 2013). We first compared the alkali-released acetic acid in the cell wall from stems of *esk1-5* and *beem396b*. As described previously, the amount of acetic acid released by *esk1-5* was significantly lower than in the wild type (Fig. 3; Xiong et al., 2013; Yuan et al., 2013). The same defect was observed in *beem396b* and in *esk1-5 kak* double mutants. In addition, the acetic acid released by *kak-7* and *kak-8* single mutants was not significantly different from that in the wild type. These results indicate that *kak* mutations have no effect on the total amount of wall-bound acetate, either in *esk1-5* or in a wild-type genetic background.

To evaluate the saccharification potential of the various mutants, cell wall residues from the two basal internodes on stems of 12-week-old plants were treated with a commercial cellulase preparation (Berthet et al., 2011). We observed that genotypes carrying both *esk1-5* and *kak* mutations released significantly more Glc than the *esk1* and *kak* single mutants or the wild-type line (Fig. 3). In contrast, neither *esk1-5* single mutants nor *kak* single mutants released more Glc than the wild type (Fig. 3). Given that it is well established that lignin has a major detrimental impact on the saccharification of plant cell walls (Chen and Dixon, 2007; Studer et al., 2011; Van Acker et al., 2013), we measured the lignin content of cell wall residues using the acetyl bromide method. The *esk1* lignin level was not significantly different from the wild-type level; similarly, the levels of the other single and double mutants were found to be not affected or affected only very weakly (Fig. 3).

To investigate if *kak* mutations have other effects on xylem cell wall composition, we then used transmission-mode Fourier transform infrared (FT-IR) microspectroscopy as described previously (Supplemental Fig. S6; Mouille et al., 2003; Lefebvre et al., 2011). The comparison curve of the statistical significance of the difference in absorbance between the wild type and the *esk1-5* mutant (Supplemental Fig. S7) showed previously reported differences (Lefebvre et al., 2011). Peaks found at 1,730, 1,369, and 1,230 cm^{-1} are located at wave numbers related to the reported infrared signature of *O*-acetyl moieties found in plant cell wall polymers: namely C=O stretching in acetyl groups (1,730 cm^{-1}), deformation of C-H linkages in the methyl group of *O*-acetyl moieties (1,369 cm^{-1}), and C=O and C-O linkages stretching vibration (1,230 cm^{-1}; Mohebby, 2008). In the right part of the spectrum, between 1,000 and 830 cm^{-1}, modifications are associated with a reduction in cellulose (Mouille et al., 2003). These results, consistent with reported *esk1-5* cell wall alterations (Lefebvre et al., 2011; Xiong et al., 2013; Yuan et al., 2013), demonstrate the accuracy of the FT-IR analysis. The comparison curves of FT-IR absorbance spectra of the hypocotyl metaxylem from *beem396b* (Supplemental Fig. S7) and *esk1-5* were very similar, as were the comparison curves from the *esk1-5 kak* double mutants and *esk1-5* (Supplemental Fig. S7). In contrast, the comparison curves of *kak-7* and *kak-8* were flat, indicating nonsignificant differences with respect to the wild type (Supplemental Fig. S7). Moreover, the gaps between *kak-7* and *kak-8* curves suggest that the detected differences were due to background noise rather than actual differences in chemical arrangement. We also analyzed the monosaccharides in cell wall residues. As described previously, the Glc mass from the cellulose fraction was significantly lower in *esk1-5* knockout genotypes (Fig. 4; Supplemental Table S2), indicating a decrease in crystalline cellulose content (Lefebvre et al., 2011; Xiong et al., 2013; Yuan et al., 2013). As reported by Xiong et al. (2013), we found more Xyl in *esk1-5* than in the wild type, but the difference was only slight and had not been observed by Yuan et al. (2013; Supplemental Table S2). We observed higher amounts of Ara, Glc, and Man (except for Man in *esk1 kak-7*) in the hemicellulose fraction from all mutants compared with the wild type, but we will not discuss these data, nor the weak differences observed in Fuc, Rha, and Gal. Released acetic acid, FT-IR profiles, and

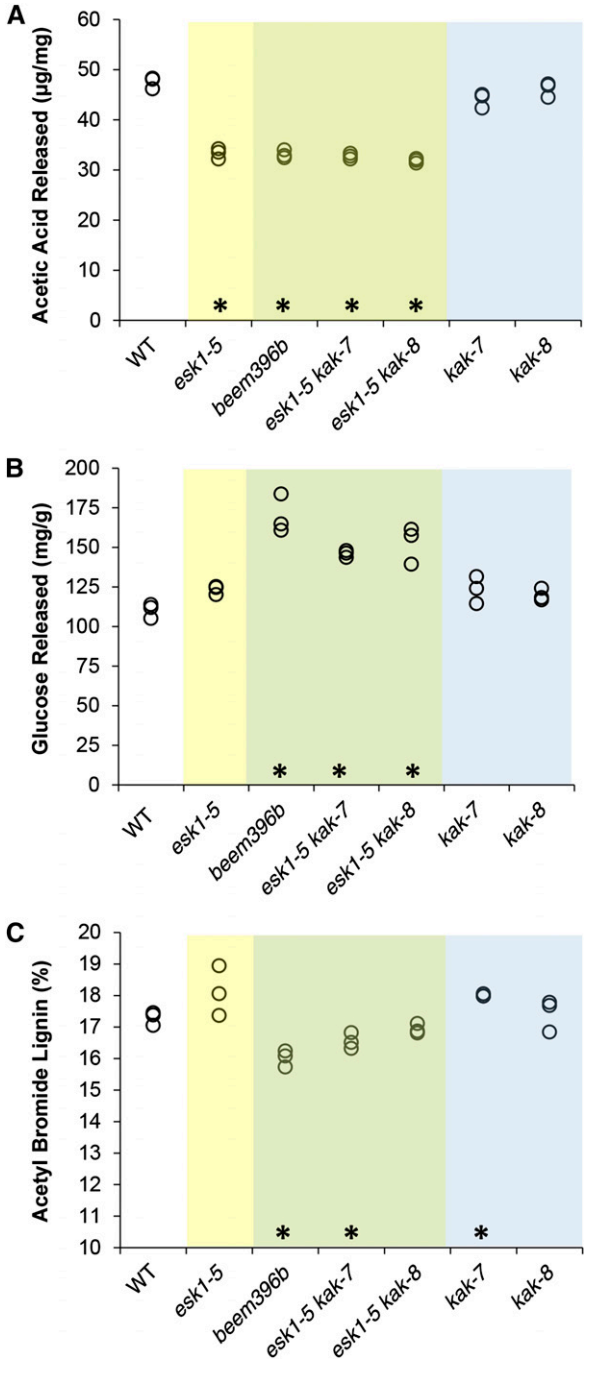

Figure 3. *esk1 kak* double mutants show higher Glc release. The same cell wall samples were analyzed for their acetate content (A), Glc release after cellulase digestion (B), and acetyl bromide lignin (C). The values of three biological replicates are shown (circles). Data from genotypes carrying the *esk1* mutation are presented on a yellow background, data from genotypes carrying the *esk1* and *kak* mutations on a green background, and data from genotypes carrying the *kak* mutation on a blue background. Asterisks over the *x* axis indicate statistically significant differences compared with the wild type (WT; Dunnett's test, $P < 0.05$; $n = 3$).

the monosaccharide analysis all suggest that *kak* mutations did not affect xylem cell wall composition in the wild type or in the *esk1-5* background. As a result, the suppression of dwarfism in *beem* and *esk1-5 kak* double mutants cannot be associated with the recovery of *O*-acetylation or any other major cell wall modifications in xylem.

The Suppression of Dwarfism Is Associated with the Recovery of Xylem Morphology

esk1-5 dwarfism is associated with an impairment of water transport due to the deformation of xylem vessels (Lefebvre et al., 2011). Observation with a light microscope of Toluidine Blue Orange-stained cross sections of 10-week-old, fully developed stem bases showed a clear suppression of the *irx* phenotype in *beem396b* (Fig. 5). Based on the measurement of 10 to 20 xylem vessel surface areas in 19 to 21 different poles from six different plants (2,299 data points; Supplemental Fig. S8), we observed a bimodal distribution (Supplemental Fig. S9). Consequently, the data were analyzed for two populations: those with large vessels and those with medium-sized vessels. Overall, we observed a pole effect in individual plants and a plant effect in genotypes. Because vessel area was heteroscedastic, we compared vessel area between genotypes with nonparametric tests (permutation-based pairwise Student's *t* tests). *beem396b* presents wild-type-like round-shaped vessels of area intermediate between *esk1-5* and the wild type in the large vessel as well as the medium vessel populations (Fig. 5; Supplemental Fig. S9). The double mutants *esk1-5 kak-7* and *esk1-5 kak-8* also showed suppression of the *irx* phenotype (Fig. 5), with round-shaped vessels showing an area similar to the wild type, in the large vessel as well as the medium vessel populations (Fig. 5; Supplemental Fig. S9). For *kak-7* and *kak-8* mutants, the vessel area distribution was large, heteroscedastic, and not significantly different from the wild type, but there was a trend toward higher vessel area, as observed with the wide range of values from the median to the third quartile. These results suggest that rosette enlargement in *beem396b* and in *esk1-5 kak* double mutants is associated with the recovery of xylem function. However, the proportion of xylem relative to phloem in the vascular pole area was not significantly different within genotypes (Fig. 5). This recovery of xylem morphology can be viewed as an increase in water transport capacity, which may account for the suppression of dwarfism in the *beem* line.

kak Partially Restores Hydraulic Conductivity

To check if suppression of the *irx* phenotype was associated with the recovery of sap flow capacity, we measured stem hydraulic conductivity. This trait was measured in segments of basal inflorescence stems sequentially shortened from 8 to 1.5 cm long (Fig. 6). In all samples, conductivity increased with stem segment

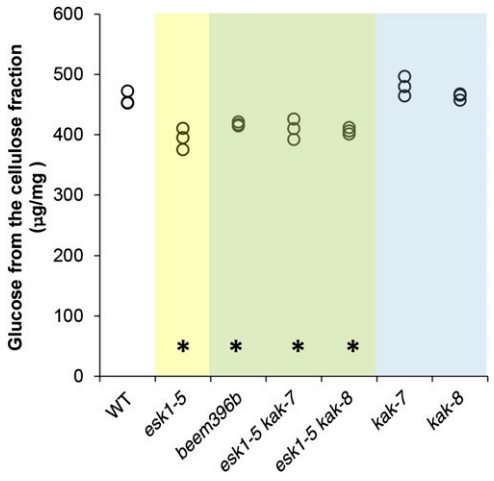

Figure 4. *kak* does not suppress the cellulose content of *esk1-5*, as indicated by Glc dosage from the cellulose fraction. The values of three biological replicates are shown (circles). Data from genotypes carrying the *esk1* mutation are shown on a yellow background, data from genotypes carrying the *esk1* and *kak* mutations on a green background, and data from genotypes carrying the *kak* mutation on a blue background. Asterisks over the *x* axis indicate statistically significant differences compared with the wild type (WT; Dunnett's test, $P < 0.05$; $n = 3$).

length, although it is the conductance normalized for length. However, stems have stomata and ramifications, and these features caused leaks in the samples. The volume of these leaks (and thus the relative amount of sap flow) increased with increasing segment length. Conductivity in *esk1-5* was significantly lower than in the other genotypes. This difference was found regardless of segment length, ruling out a length effect ($P < 0.05$ for the *esk1-5* effect in a two-way ANOVA, genotype × segment length). *esk1* mutants are known to have low hydraulic conductivity (Lefebvre et al., 2011). The wild-type genotype had the highest conductivity, which was not significantly different in *kak* single and *esk1-5 kak* double mutants, due to high variance. Nevertheless, for each segment length (except 8 cm), a multiple pairwise comparison test (Tukey's test, $P < 0.05$) clustered *kak* mutants and *esk1-5 kak* double mutants, with *beem396b* as intermediate to the *esk1-5* single mutant and the wild type.

KAK Is Expressed in Vascular Tissues

In *kak* mutants, stem diameter was about 30% larger than in the wild type, consistent with the recovery of stem diameter found in *beem396b* (Fig. 1). In *esk1 kak* double mutants, xylem vessels had a round shape, testifying to the absence of collapsed xylem vessels. This suggests a possible involvement of *KAK* in secondary growth and/or vascular patterning. To investigate this possibility, we used the *GUS* reporter gene to study the *KAK* gene expression pattern. A 2-kb sequence upstream from the *KAK* gene transcription starting site (KAK_{pro}) was fused with the *GUS* reporter gene. Examination of GUS activity in wild-type plants transformed with the KAK_{pro}:*GUS* construct showed specific expression in leaf vascular tissues, root tips, and emerging lateral roots of 14-d-old plants (Fig. 7). In fully developed, flowering 8-week-old transgenic plants, GUS activity was detected in reproductive organs (i.e. pollen grains, ovules, and seeds; Fig. 7). Observation of hypocotyl cross sections with a light microscope showed specific GUS activity in the vascular cambium, the meristematic zone that gives rise to secondary phloem and xylem. GUS activity was also observed in the hypocotyl near the cambium on the phloem side and possibly in young secondary xylem cells, although the latter two cell types are difficult to identify because they are small and undifferentiated (Fig. 8; Ye et al., 2002; Turner and Sieburth, 2003). In stem vascular bundles, strong GUS activity was found in the phloem, in the cambium, and in the primary xylem, in cells surrounding the vessels (Fig. 8). The *KAK* gene expression pattern, as shown via GUS activity, indicated that *KAK* may play a role in vascular development as well as in male gametophytes, ovules, and developing seeds.

The observed *KAK* expression pattern in vascular tissues, therefore, was consistent with the suppressed *irx* phenotype in *esk1 kak* double mutants.

DISCUSSION

The Suppression of the Small Rosette Size in *esk1-5* Is Indirect

ESK1/TBL29 has *O*-acetyltransferase activity that operates in xylem tissues (Xiong et al., 2013; Yuan et al., 2013; Urbanowicz et al., 2014). The absence of this function is associated with an *irx* phenotype; consequently, the *esk1* knockout mutants show reduced hydraulic conductivity and dwarfism (Lefebvre et al., 2011). Thus, the suppression of the *esk1* dwarf phenotype may be due either to the recovery of xylem function or to an indirect compensatory growth effect.

According to our study, the suppression of the *esk1* dwarf phenotype in the *beem396b* line results from the inactivation of the *KAK* gene. The effect of *kak* mutations in *beem396b* suggests that the effect of the suppression of dwarfism is indirect. *kak* mutants have previously been described as affecting trichome morphology (Perazza et al., 1999). As expected, *beem396b* and *esk1 kak* double mutants both present overbranched trichomes, similar to single insertional *kak* mutants (Supplemental Fig. S3). *beem396b* has larger metaxylem vessel areas than *esk1-5* but smaller than the wild type, probably due to other, undesirable mutations (Fig. 5). The *esk1 kak* double mutants have a round shape and larger metaxylem vessel area than *esk1*, causing the suppression of the *irx* phenotype (Fig. 5). However, there were no differences in the proportion of the xylem area in fascicular bundles among genotypes (Fig. 5), in accordance with normally coordinated vascular development. Our data are consistent with the previous hypothesis that the collapsed xylem (*irx*) phenotype causes dwarfism and impairs

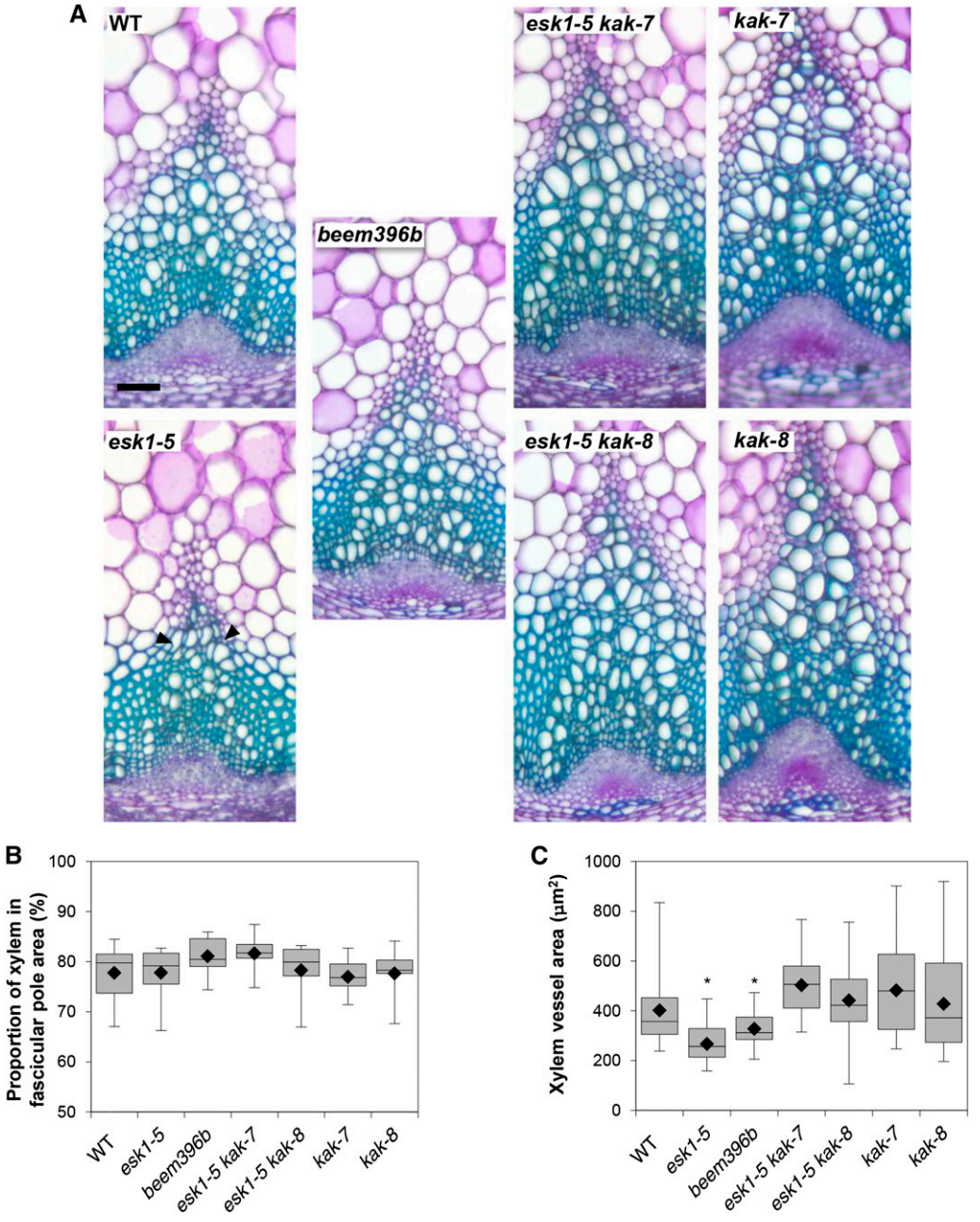

Figure 5. *kak* mutations have an effect on xylem morphology. A, Cross sections of stem vascular bundles stained with Toluidine Blue. WT, Wild type. Black arrowheads indicate collapsed xylem vessels. Bar = 50 mm. B, Proportion of xylem in the vascular pole area. For each genotype, the areas of xylem and phloem in the fascicular poles from six independent plants were measured as described in Supplemental Figure S8. C, Xylem vessel surface area. Vessel area (from the largest vessel population) measurements were taken for each genotype on 19 to 21 different xylem poles from six independent plants, as described in Supplemental Figure S8. For the box and whisker plots (B and C), black diamonds represent the means, lines in boxes represent medians, top and bottom ends of the boxes represent the first and third quartiles, respectively, and whisker extremities represent maximum and minimum data points. Asterisks indicate the genotypes that are significantly different from the other genotypes ($P < 0.05$), as attested by pairwise permutational Student's *t* tests (999 permutations).

water uptake from the soil to the aerial organs (Lefebvre et al., 2011). Moreover, the reverse relationship also appears to hold: the suppression of the *irx* phenotype partially suppresses the dwarf phenotype and restores hydraulic conductivity. The fact that the chemical composition of *beem396b* is similar to that of genotypes carrying the *esk1* mutation, and that the chemical composition of *kak* mutants is similar to the wild type, confirms this indirect suppression (Figs. 3 and 4; Supplemental Fig. S7). The biological system of the *esk1*

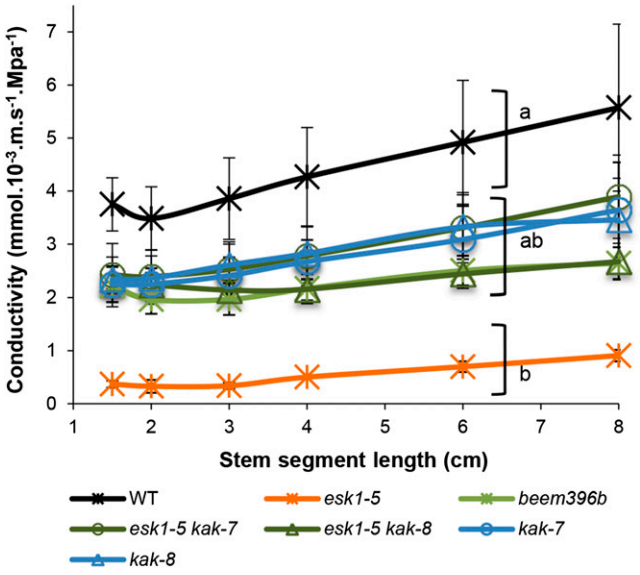

Figure 6. *kak* partially suppress the conductivity default of *esk1-5*. Hydraulic conductivity was measured on segments of basal inflorescence stems sequentially shortened and plotted as a function of segment length. Each data point represents the mean of two (*esk1-5*) to six biological replicates. Brackets with different letters indicate genotype groups that are significantly different ($P < 0.1$), for each segment length except 8 cm, according to Tukey's multiple pairwise comparisons test. Error bars indicate SE. WT, Wild type.

mutant and its suppressor lines are valuable tools for identifying major genes involved in diverse functions related to water fluxes in planta.

Although *kak* mutations appear to have no major impact on xylem cell wall composition, the issue of the suppression mechanism of the *irx* phenotype nevertheless remains. Yuan et al. (2013) attributed the collapsed xylem phenotype of *esk1* not only to chemical alterations but also to a reduction in secondary cell wall thickening, which is consistent with a decrease in cellulose content. Thus, a possible explanation for *irx* suppression by *kak* mutations involves the recovery or enhancement of secondary cell wall thickening in xylem. However, we did not observe any recovery of cellulose content and only a partial recovery of hydraulic conductivity. Further characterization of *esk1-5 kak* xylem cell walls with transmission electron microscopy can address the question of secondary wall thickening. Hydraulic conductivity not only depends on vessel diameter and number but on resistance to water flow in the vessel end walls. This latter component of hydraulic conductivity is a function of vessel length and intervessel pits that form thin-walled areas, allowing sap flow between vessels. Thus, a comprehensive study requires a correlation analysis of structural, chemical, and functional parameters. Moreover, vulnerability to cavitation is another avenue for investigation, because this trait relies on vessel structure and is involved in drought tolerance (Tixier et al., 2013).

KAK May Be Involved in Vascular Development

We described new, clear-cut effects of *kak* inactivation on vascular morphology in an *esk1-5* genetic background. *kak* single mutants show amplified stem diameter (Fig. 1), and the xylem vessel population is made up of larger tracheary elements (Fig. 5). *KAK* is expressed in trichomes, cotyledons, and roots in 4-d-old plantlets (Patra et al., 2013). We also observed that

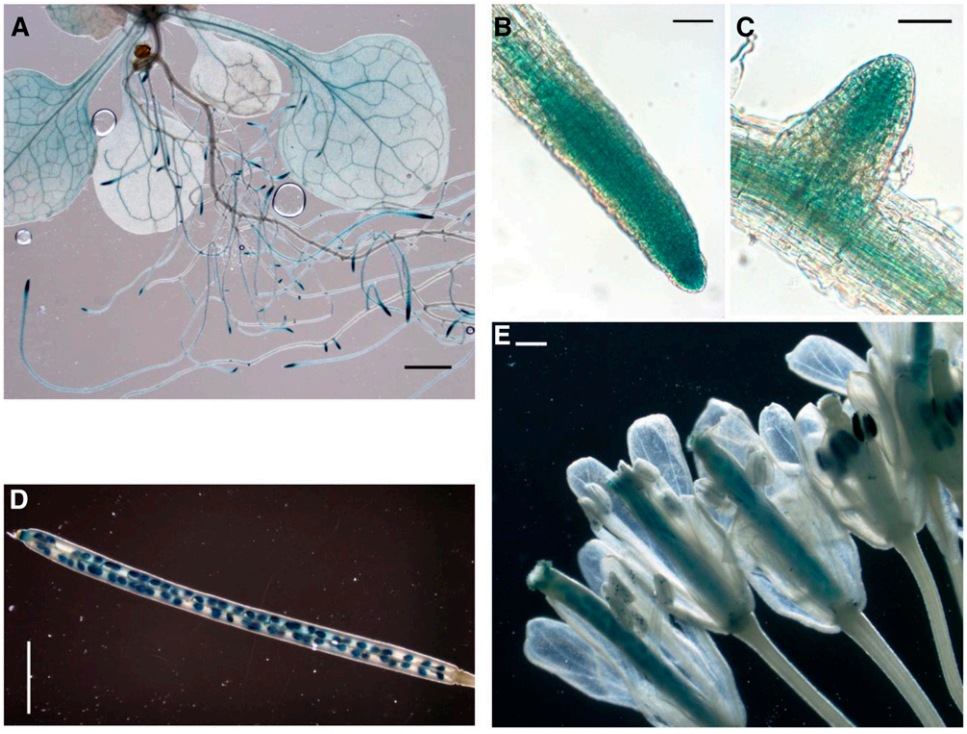

Figure 7. Expression of KAK_{pro}:*GUS* in vascular tissues, root tips, pollen, ovaries, and seeds. A to C, Fifteen-day-old seedling. A, Observation with a stereomicroscope of a plantlet showing expression in vascular tissues. Bar = 200 mm. B and C, Observation with a light microscope of a root tip (B) and an emerging lateral root (C) with expression in meristems. Bars = 1 mm. D and E, Eight-week-old flowering plant. D, Maturing siliques showing expression in seeds. Bar = 1 mm. E, Fully developed flower showing expression in ovules and pollen grains. Bar = 100 mm.

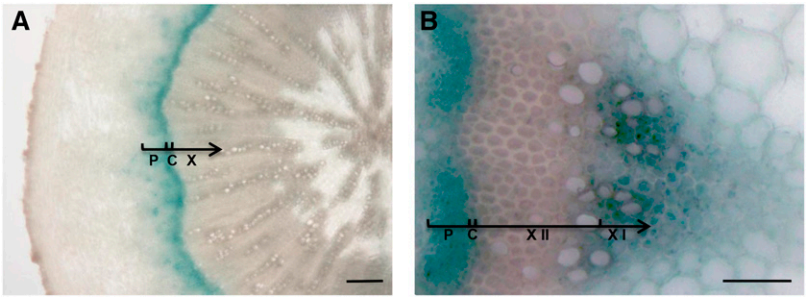

Figure 8. Expression of KAK_{pro}:*GUS* in the xylem, cambium, and phloem. Hypocotyl (A) and stem (B) cross sections were observed with a light microscope. Phloem (P), cambium (C), xylem (X), secondary xylem (X II), and primary xylem (X I) are indicated. Bars = 20 μm (A) and 5 μm (B).

KAK_{pro} drives gene expression in the vascular cambium, phloem, and primary xylem (Fig. 8). Its expression in cambium, which is the secondary meristem that gives rise to both secondary xylem and the phloem, leads to the hypothesis that KAK may play a role in the balance between xylem and phloem formation. KAK is described as an endoreduplication repressor (Downes et al., 2003; El Refy et al., 2003): it may control cell enlargement in both xylem and phloem, acting with different partners. For example, it interacts with GLABROUS3 (GL3) and ENHANCER OF GLABROUS3 (EGL3) in leaf epidermal cells to repress trichome formation by targeting its partners for the proteasome (Patra et al., 2013). GL3 is also involved in root hair formation through an activation/repression cascade similar to the one involved in epidermal cell differentiation that leads to trichome formation (Ishida et al., 2008). However, we measured root hair length and density in the wild type, *esk1-5*, *beem396b*, *esk1-5 kak* double mutants, and *kak* single mutants, and there was no genotype effect. Additional evidence provides support for *KAK* effects in cells other than trichomes. For example, *kak* mutants exhibit an enhanced endoreduplication level in etiolated hypocotyls, which completely lack trichomes (El Refy et al., 2003), suggesting that *KAK* plays a broad role in the plant wherever the control of endoreduplication is required. The intense GUS activity in root tips and lateral root primordia (Fig. 7) suggests that KAK is also expressed in apical meristems. In addition, KAK activity occurs in ovules, pollen, and maturing seeds (Fig. 7): cell division versus endoreduplication is probably tightly regulated in these types of cells.

However, it has not yet been demonstrated if the control of endoreduplication by KAK in trichomes is mediated by the degradation of GL3. The possibility that KAK interacts with other target(s) to control endoreduplication through a yet unknown pathway cannot be ruled out. Addressing this issue requires an analysis of *esk1 kak gl3* triple mutants.

KAK recognizes the GL3/EGL3/GL1 complex to be degraded by the 26S proteasome, activating *GL2* in trichomes, which in turn represses *CELLULOSE SYNTHASE5* (*CESA5*) and activates *XYLOGLUCAN ENDOTRANSGLUCOSYLASE17* (*XTH17*), two genes annotated as being involved in cell wall biogenesis and cell wall organization, respectively (Tominaga-Wada et al., 2009). Currently, we cannot discount the possibility that *kak* inactivation interferes with this cascade to suppress *esk1* dwarfism. Nevertheless, *cesa5* mutants have a seed mucilage phenotype (Sullivan et al., 2011), and vegetative plants are indistinguishable from the wild type (Desprez et al., 2007). *XTH17* is expressed mostly in roots (Vissenberg et al., 2005; Becnel et al., 2006). Furthermore, our FT-IR and monosaccharide analyses do not support this hypothesis of KAK involvement in cell wall processes, because the results did not show any major differences in cell wall composition or between *esk1*, *beem396b*, *esk1 kak-7*, and *esk1 kak-8*.

esk1 beem Double Mutants Are Potentially Valuable Genotypes

beem396b and *esk1 kak* double mutants did not appear to show any cell wall modifications compared with *esk1*: their FT-IR profiles were similar, and they released less acetate than the wild type, similar to *esk1-5*. This similarity is consistent with ESK1 having xylan acetyltransferase enzymatic activity and with KAK having no effect on cell wall composition. Nonetheless, *beem396b* and *esk1 kak* double mutants are larger than *esk1-5* mutants. *esk1 kak* and other *beem* lines may be regarded as potentially valuable genotypes, considering their vegetative size, which is close to that of the wild type (Fig. 1), and their lower acetate release (Fig. 3).

We observed enhanced saccharification of cell wall residues from mature 12-week-old stems in *esk1 kak* double mutants compared with the wild type and *esk1* or *kak* single mutants (Fig. 3). This enhanced saccharification cannot be clearly attributed to a lower lignin level (Fig. 3). The recalcitrance of lignified cell walls to saccharification has a multifactorial origin, and another compositional trait of Arabidopsis cell walls may have a lower degree of acetylation, thus facilitating polysaccharide enzymatic hydrolysis (for review, see Pawar et al., 2013). The lower acetylation level in polymers has been described as beneficial for polymer degradation: polymers are more accessible to degrading enzymes, and degradation is more effective. Stem acetylation is reduced in the *esk1* single and double mutants (Xiong et al., 2013). This reduced acetylation is associated with the improved enzymatic degradability

of cell wall polysaccharides for the *esk1 kak* double mutants but not for the dwarf *esk1* single mutant. Xiong et al. (2013) reported lower Glc yields for the *esk1* mutant in a saccharification assay performed on destarched alcohol-insoluble residues obtained from 7-week-old stems. However, the saccharification conditions employed in that study led to very low Glc yields (close to 20 mg g^{-1} destarched alcohol-insoluble residues), in contrast to the 5- to 8-fold higher yield obtained in our study. Variation among samples, due to sampling and processing, is very likely responsible for the apparent differences in saccharification performance in the *esk1* single mutant. We cannot conclude from our study that acetylation degree is associated with saccharification yield. However, *esk1* is severely affected regarding stature, stem mechanical strength, secondary wall thickening (Yuan et al., 2013), and crystalline cellulose content (Lefebvre et al., 2011). These physical and chemical alterations may impair Glc release. Further investigations need to be done to explore saccharification.

Nevertheless, *esk1 kak* double mutants retain both the advantages of releasing less acetate but more Glc, on the one hand, and having a large vegetative size, on the other hand.

Here, KAK was identified as a suppressor of dwarfism and the collapsed xylem phenotype observed in *esk1*. Further investigations are required to determine the mechanism behind this suppression. Endoreduplication is currently being explored for its potential involvement in vascular formation. Other mechanisms that may result in cell wall thickening in xylem vessels are also being considered.

The *esk1* mutant has a permanent drought syndrome (Bouchabke-Coussa et al., 2008). Given the restored xylem vessel morphology and the partially restored hydraulic conductivity reported in *esk1 kak* double mutants, it is worth exploring the drought response in *beems*, *esk1 kak* double mutants, as well as *kak* single mutants.

MATERIALS AND METHODS

Screening for *esk1-5* Mutant Dwarfism Suppressors (*beems*)

EMS mutagenesis of Arabidopsis (*Arabidopsis thaliana*) seeds from the *esk1-5* mutant (SALK_089531) was performed according to a previously described protocol (Lightner and Caspar, 1998). About 4,500 M1 plants of the resulting mutagenized population were pooled into bulks of seven plants and advanced to the M2 generation. For each bulk, 200 M2 plants were screened for rosette size compared with *esk1-5* in a greenhouse. Theoretically, three to four plants with a suppressed *esk1-5* phenotype were expected in a bulk, if one of the seven lines harbored a single recessive causative mutation (Page and Grossniklaus, 2002). Phenotype stability of the *beem* lines isolated in the M2 population was checked in their M3 progeny and selected if stable. Selected M2 *beem* lines were then backcrossed twice to their mutant background *esk1-5* to segregate away some noncausative EMS-induced mutations.

Direct Mapping and Identification of the *beem396b* Causative Mutation

The F2 population resulting from the second backcross of the *beem396b* M2 line was used for mapping by sequencing. Among 570 F2 seeds sown, 124 plants with the largest rosettes were selected, of which 100 were sequenced. Genomic DNA was extracted from flowers of each F2 plant using the protocol described in Supplemental Protocol S1. Briefly, after cetyl-trimethyl-ammonium bromide-based extraction and subsequent RNase treatment, DNA was further purified with phenol-chloroform and quantified using a fluorimetrics-based method (Qubit Fluorimetric Quantification; Life Technologies; http://www.lifetechnologies.com). Equal amounts of genomic DNA from these plants were pooled and sequenced using the Illumina system (http://www.illumina.com/). The generation of sequencing libraries and sequencing were performed at the High-Throughput Sequencing Department at the IMAGIF facility (https://www.imagif.cnrs.fr/plateforme-36-High-throughput_Sequencing_Platform.html) at the Centre National de la Recherche Scientifique. Here, 2 μg of pooled DNA was used to generate a paired-end sequencing library according to Illumina's protocol. The sequencing library was sequenced using four lanes of a Genome Analyzer II_x flow cell to an expected depth of 100×. A second nonallelic *beem* line F2 population was also sequenced independently.

The obtained short sequence reads were aligned to the Arabidopsis genome (version TAIR10) to identify mutations using the Illumina package CASAVA 1.8.2., leading to 2.1×10^5 and 2.2×10^5 reads mapping unambiguously on the genome. A homemade pipeline was developed to process the CASAVA output files from both *beem* lines and identify the causative mutations using a strategy similar to that described by Hartwig et al. (2012; Supplemental Protocol S2).

Confirmation of the *beem396b* Mutation and Identification of the *beem308a* Mutation

The EMS-induced *kak* mutation in *beem396b* was confirmed by sequencing overlapping PCR products encompassing the full *KAK* genomic sequence, including a 2-kb upstream transcription start site and a 2-kb downstream transcription termination site, using the primer couples listed in Supplemental Table S1. The same primers were also used to confirm the *beem308a* mutation.

Determination of Cell Wall-Bound Acetate Content

Inflorescence stems, minus their leaves, were sampled from just above the rosette on 12-week-old greenhouse-grown plants, and all stems were cut at a height corresponding to the second internode on the main stem. Sampled stems were immediately frozen in liquid nitrogen, lyophilized, and then ground to a fine powder in a grinding machine (Mixer Mill MM-2; Retsch; http://www.retsch.com/). Each sample was extracted three times with MilliQ water and three times with 96% (v/v) ethanol at 80°C, then air dried to obtain cell wall residues. The acetate content of cell wall residues was determined using the Megazyme Acetic Acid Kit (K-ACET version 02/11; http://www.megazyme.com/). The assay was downscaled and adapted to a 96-well format and performed essentially as described previously (Gille et al., 2011), with some slight modifications as follows. A total of 2 mg of cell wall residues was suspended in 100 μL of MilliQ water. The cell wall-bound acetate was released by adding 100 μL of 1 M NaOH and incubating for 1 h at room temperature with shaking at 500 rpm. The samples were neutralized with 1 M HCl and centrifuged for 10 min at 14,000 rpm, and 10 μL of the supernatant containing released acetate was transferred to a UV light-capable, 96-well flat-bottom assay plate and diluted with 94 μL of water. The kit content was used as follows. MilliQ water and solutions 2, 3, and 4 were mixed in a ratio of 96.8:2.5:1:1 (115.6 μL + 30 μL + 1.2 μL + 1.2 μL per sample), and 148 μL of this mixture was added to each sample, mixed, and incubated at room temperature for 2 min. The absorbance was read at 340 nm. Solution 5 was diluted 1:10 in water; 12 μL was added to each sample, mixed, and incubated at room temperature for 4 min. The absorbance was read at 340 nm. The amount of acetate in the samples was calculated based on an acetic acid standard curve and according to the manufacturer's recommendations.

Evaluation of Cell Wall Lignin Content and Enzymatic Degradability

The lignin content of the same cell wall residues used for acetate determination was measured as acetyl bromide lignin and according to a procedure adapted from Fukushima and Hatfield (2001). In brief, 5 to 6 mg of cell wall residues weighed to the nearest 0.01 mg was mixed with 1 mL of freshly prepared 25% (v/v) acetyl bromide in acetic acid in a 2-mL glass vial with a Teflon-lined screw cap. The mixture was then allowed to digest in a thermomixer operated at 55°C

and at 600 rpm for 150 min. After cooling, 100 μL of the reaction supernatant was transferred into a 5-mL disposable glass tube together with 1.5 mL of acetic acid:2 M NaOH (50:9, v/v). Then, 0.4 mL of 0.5 M hydroxylamine chlorohydrate and 1 mL of acetic acid were added. The absorbance of the solution was read at 280 nm against a reagent blank. Acetyl bromide lignin content was calculated from this absorbance using an extinction coefficient of 20 g^{-1} L cm^{-1}. The measurements were performed from biological triplicates.

The enzymatic degradability of the cell wall residues was measured according to a procedure adapted from Berthet et al. (2011). Briefly, 25 to 30 mg of sample weighed to the nearest 0.1 mg was put in a 5-mL disposable plastic tube together with 4 mL of 0.05 M acetate buffer, pH 4.7, containing 4 mg mL^{-1} of a commercial cellulase preparation (cellulase Onozuka R-10 from *Trichoderma viride*; Serva) and 0.2 mg mL^{-1} NaN_3. A reagent blank was prepared without cell wall residues. The reaction tubes (biological triplicates for each genotype plus the reagent blank) were placed on a carousel at 45°C for 60 h and then centrifuged (1,500*g*, 10 min). The Glc released into the reaction mixture was measured using the Biomerieux Glc RTU kit as follows. In a disposable 1-mL spectrophotometry cuvette, 50 μL of the supernatant was mixed with 1 mL of the Biomerieux reagent, and the colorimetric reaction was allowed to proceed for 30 min. Absorbance was read at 505 nm against a cuvette containing 50 μL of water and 1 mL of reagent. This absorbance was corrected for the absorbance obtained for the reagent blank (i.e. for the Glc originating from the Onozuka cellulase preparation). The Glc amounts released by enzymatic hydrolysis of the extract-free samples were calculated after appropriate calibration with standard Glc solutions (prepared in the 0.2–1 mg mL^{-1} range).

Neutral monosaccharide composition was measured as indicated (Simons et al., 2014).

Hydraulic Conductivity

For hydraulic analyses, seeds were sown on a commercial soil mixture (Humustar) and grown in a growth chamber at 22°C to 20°C under a light intensity of 100 μmol m^{-2} s^{-1} (16-h-light/8-h-dark cycle) and with 60% relative humidity. As soon as inflorescence stems showed ripening siliques (i.e. after 7–8 weeks), they were harvested and immediately used for analysis. Hydraulic conductivity (m^4 MPa^{-1} s^{-1}) was measured on segments of basal inflorescence stems using a Xyl'em apparatus (Bronkhorst). Stem segments 8 cm long were cut under water to avoid embolism. Then, the basal ends were gently sealed in a tubing system using seal tape (polytetrafluoroethylene film) to avoid leaking and crushing the samples with the clamps. A solution of KCl (10 mM) and $CaCl_2$ (1 mM) was used to perfuse stems basipetally under 6 to 9 kPa at room temperature, and the flow rate was scored 3 min after starting the perfusion. To evaluate the effect of segment length on conductivity, the stem segment was shortened at its end apex to 6, 4, 3, 2, and 1.5 cm, and the flow rate was measured at each length.

Analysis of *KAK* Promoter Expression Pattern

The expression pattern of the *KAK* gene was studied using the *GUS* reporter gene. A 2-kb sequence upstream from the *KAK* gene transcription starting site was amplified from wild-type genomic DNA using *att*B-flanked primers for subsequent Gateway cloning (primers are listed in Supplemental Table S1). The PCR product was first cloned into a pDONR207 vector (Invitrogen; http://www.lifetechnologies.com) with a BP reaction and transferred using an LR reaction into pBI101-R2R3-GUS, a Gateway-compatible binary vector derived from pBI101 (Harscoët et al., 2010), to generate a transcriptional fusion between the *KAK* promoter (KAK_{pro}) and the *GUS* reporter gene. The KAK_{pro}:*GUS* construct was introduced into wild-type plants by *Agrobacterium tumefaciens*-mediated transformation as described previously (Bechtold and Pelletier, 1998). Eight independent transformed lines with nonsegregating insertions were selected on kanamycin and used for GUS activity assay. The GUS activity assays were performed as reported previously (Marrocco et al., 2003). The eight independent KAK_{pro}:*GUS*-transformed lines tested showed similar GUS activity patterns.

Cytology and Microscopy

Trichomes were observed on the fourth true leaves of 14-d-old in vitro-grown plants using an SH-1500 scanning electron microscope (Hirox Europe; http://www.hirox-europe.com/).

For Toluidine Blue Orange staining and FT-IR analysis, hypocotyls were collected from 10-week-old greenhouse-grown plants and cleared in 96% (v/v) ethanol. After rehydration, samples were directly glued to a vibratome-compatible disk and cut while immersed in water. The thickness of the cross sections was 20 μm.

Stem basal internodes and hypocotyls were collected from 8-week-old greenhouse-grown plants transformed with the KAK_{pro}:*GUS* construct.

FT-IR Microspectroscopy

FT-IR analysis on hypocotyl cross sections was performed as described previously (Lefebvre et al., 2011) with the following modifications. The cross section thickness was 20 μm, and the acquisition window of the microspectrophotometer was set to 40 $\times$ 40 μm. For each genotype, a total of 45 spectra were acquired from three independent plants. The zone targeted for the acquisition of spectra was the upper region of metaxylem as shown in Supplemental Figure S7.

Statistical and Image Analyses

Statistical analyses were performed using R (http://www.r-project.org/). Nonparametric tests were performed using the packages nparcomp for Tukey's or Dunnett's tests (Konietschke et al., 2012) and RVAideMemoire for tests with permutations (Hervé, 2014). Measurements on images were performed with the ImageJ software (http://rsbweb.nih.gov/ij/).

The genetic background of every plant line studied here was Columbia-0. Two independent T-DNA mutants with insertion sites within the *KAK/UPL3* gene (At4g38600) were ordered from the Salk Institute Genomic Analysis Laboratory collection. T-DNA mutants were named *kak-7* (SALK_116326) and *kak-8* (SALK_117247). *kak* homozygous T-DNA lines were identified by PCR using gene- and T-DNA-specific primers obtained using the T-DNA Primer Design tool provided by the Salk Institute Genomic Analysis Laboratory (http://signal.salk.edu/tdnaprimers.2.html). Primer sequences are listed in Supplemental Table S1.

The Arabidopsis Genome Initiative locus identifier of the *ESK1/TBL29* gene is At3g55990. The sequence data mentioned here can be found in the GenBank data libraries under project accession number PRJNA253006 and sample accession number SAMN02869710.

Supplemental Data

The following supplemental materials are available.

Supplemental Figure S1. Mapping of EMS mutation frequency in a *beem396b* pool.

Supplemental Figure S2. Effect of the *beem396b* mutation within the *KAK* coding sequence.

Supplemental Figure S3. Scanning electron micrographs of leaf trichomes.

Supplemental Figure S4. *beem308a* has a lesion in the *KAK* gene.

Supplemental Figure S5. Reverse transcription-PCR detection of an *ESK1* transcript.

Supplemental Figure S6. Zone targeted for FT-IR microspectroscopy.

Supplemental Figure S7. FT-IR analysis of metaxylem vessels.

Supplemental Figure S8. Measurements of xylem pole, phloem pole, and xylem vessel area.

Supplemental Figure S9. Metaxylem vessel area distribution and analysis.

Supplemental Table S1. List of PCR primers.

Supplemental Table S2. Cell wall monosaccharides.

Supplemental Protocol S1. Preparation and pooling of genomic DNA for Illumina deep sequencing.

Supplemental Protocol S2. High-output sequencing analysis.

ACKNOWLEDGMENTS

We thank Salem Chabout and Halima Morin for assistance in FT-IR analysis and microscopy, respectively; the Observatoire du Végétal/Centre de Ressources *Arabidopsis thaliana* team for assistance in screening for the *beem* lines; Liudmila Chelysheva for image processing; Florian Deligne for mutant

genotyping and image analysis; and Herman Höfte, Samantha Vernettes, and Matthieu Reymond for critical reading of the article.

Received January 27, 2015; accepted April 15, 2015; published April 17, 2015.

LITERATURE CITED

Abe A, Kosugi S, Yoshida K, Natsume S, Takagi H, Kanzaki H, Matsumura H, Yoshida K, Mitsuoka C, Tamiru M, et al (2012) Genome sequencing reveals agronomically important loci in rice using MutMap. Nat Biotechnol **30:** 174–178

Bechtold N, Pelletier G (1998) In planta Agrobacterium-mediated transformation of adult Arabidopsis thaliana plants by vacuum infiltration. Methods Mol Biol **82:** 259–266

Becnel J, Natarajan M, Kipp A, Braam J (2006) Developmental expression patterns of Arabidopsis XTH genes reported by transgenes and Genevestigator. Plant Mol Biol **61:** 451–467

Berthet S, Demont-Caulet N, Pollet B, Bidzinski P, Cézard L, Le Bris P, Borrega N, Hervé J, Blondet E, Balzergue S, et al (2011) Disruption of *LACCASE4* and *17* results in tissue-specific alterations to lignification of *Arabidopsis thaliana* stems. Plant Cell **23:** 1124–1137

Biely P (1985) Microbial xylanolytic system. Trends Biotechnol **3:** 286–289

Bouchabke-Coussa O, Quashie ML, Seoane-Redondo J, Fortabat MN, Gery C, Yu A, Linderme D, Trouverie J, Granier F, Téoulé E, et al (2008) ESKIMO1 is a key gene involved in water economy as well as cold acclimation and salt tolerance. BMC Plant Biol **8:** 125–148

Buvat R (1989) Ontogeny, Cell Differentiation, and Structure of Vascular Plants. Springer-Verlag, Berlin

Chen F, Dixon RA (2007) Lignin modification improves fermentable sugar yields for biofuel production. Nat Biotechnol **25:** 759–761

Desprez T, Juraniec M, Crowell EF, Jouy H, Pochylova Z, Parcy F, Höfte H, Gonneau M, Vernhettes S (2007) Organization of cellulose synthase complexes involved in primary cell wall synthesis in Arabidopsis thaliana. Proc Natl Acad Sci USA **104:** 15572–15577

Downes BP, Stupar RM, Gingerich DJ, Vierstra RD (2003) The HECT ubiquitin-protein ligase (UPL) family in Arabidopsis: UPL3 has a specific role in trichome development. Plant J **35:** 729–742

Ebringerova A, Heinze T (2000) Xylan and xylan derivatives: biopolymers with valuable properties. I. Naturally occurring xylans structures, isolation procedures and properties. Macromol Rapid Commun **21:** 542–556

El Refy A, Perazza D, Zekraoui L, Valay JG, Bechtold N, Brown S, Hülskamp M, Herzog M, Bonneville JM (2003) The Arabidopsis KAKTUS gene encodes a HECT protein and controls the number of endoreduplication cycles. Mol Genet Genomics **270:** 403–414

Esau K (1965) Anatomy of Seed Plants, Ed 2. John Wiley & Sons, New York

Faik A (2010) Xylan biosynthesis: news from the grass. Plant Physiol **153:** 396–402

Fukushima RS, Hatfield RD (2001) Extraction and isolation of lignin for utilization as a standard to determine lignin concentration using the acetyl bromide spectrophotometric method. J Agric Food Chem **49:** 3133–3139

Gille S, Cheng K, Skinner ME, Liepman AH, Wilkerson CG, Pauly M (2011) Deep sequencing of voodoo lily (Amorphophallus konjac): an approach to identify relevant genes involved in the synthesis of the hemicellulose glucomannan. Planta **234:** 515–526

Grohmann K, Mitchell DJ, Himmel ME, Dale BE, Schroeder HA (1989) The role of ester groups in resistance of plant cell wall polysaccharides to enzymatic hydrolysis. Appl Biochem Biotechnol **20/21:** 45–61

Harscoët E, Dubreucq B, Palauqui JC, Lepiniec L (2010) NOF1 encodes an Arabidopsis protein involved in the control of rRNA expression. PLoS ONE **5:** e12829

Hartwig B, James GV, Konrad K, Schneeberger K, Turck F (2012) Fast isogenic mapping-by-sequencing of ethyl methanesulfonate-induced mutant bulks. Plant Physiol **160:** 591–600

Hervé M (2014) RVAideMemoire: diverse basic statistical and graphical functions. R package version 0.9-41. http://CRAN.R-project.org/package=RVAideMemoire (March 14, 2015)

Ishida T, Kurata T, Okada K, Wada T (2008) A genetic regulatory network in the development of trichomes and root hairs. Annu Rev Plant Biol **59:** 365–386

Konietschke F, Libiger O, Hothorn LA (2012) Nonparametric evaluation of quantitative traits in population-based association studies when the genetic model is unknown. PLoS ONE **7:** e31242

Lefebvre V, Fortabat MN, Ducamp A, North HM, Maia-Grondard A, Trouverie J, Boursiac Y, Mouille G, Durand-Tardif M (2011) ESKIMO1 disruption in Arabidopsis alters vascular tissue and impairs water transport. PLoS ONE **6:** e16645

Lightner J, Caspar T (1998) Seed mutagenesis of Arabidopsis. Methods Mol Biol **82:** 91–103

Lugan R, Niogret MF, Kervazo L, Larher FR, Kopka J, Bouchereau A (2009) Metabolome and water status phenotyping of Arabidopsis under abiotic stress cues reveals new insight into ESK1 function. Plant Cell Environ **32:** 95–108

Marrocco K, Lecureuil A, Nicolas P, Guerche P (2003) The Arabidopsis SKP1-like genes present a spectrum of expression profiles. Plant Mol Biol **52:** 715–727

Mohebby B (2008) Application of ATR infrared spectroscopy in wood acetylation. J Agric Sci Technol **10:** 253–259

Mouille G, Robin S, Lecomte M, Pagant S, Höfte H (2003) Classification and identification of Arabidopsis cell wall mutants using Fourier-transform infrared (FT-IR) microspectroscopy. Plant J **35:** 393–404

Page DR, Grossniklaus U (2002) The art and design of genetic screens: Arabidopsis thaliana. Nat Rev Genet **3:** 124–136

Patra B, Pattanaik S, Yuan L (2013) Ubiquitin protein ligase 3 mediates the proteasomal degradation of GLABROUS 3 and ENHANCER OF GLABROUS 3, regulators of trichome development and flavonoid biosynthesis in Arabidopsis. Plant J **74:** 435–447

Pawar PM, Koutaniemi S, Tenkanen M, Mellerowicz EJ (2013) Acetylation of woody lignocellulose: significance and regulation. Front Plant Sci **4:** 118

Perazza D, Herzog M, Hülskamp M, Brown S, Dorne AM, Bonneville JM (1999) Trichome cell growth in Arabidopsis thaliana can be derepressed by mutations in at least five genes. Genetics **152:** 461–476

Ragni L, Nieminen K, Pacheco-Villalobos D, Sibout R, Schwechheimer C, Hardtke CS (2011) Mobile gibberellin directly stimulates *Arabidopsis* hypocotyl xylem expansion. Plant Cell **23:** 1322–1336

Simons M, Saha R, Amiour N, Kumar A, Guillard L, Clément G, Miquel M, Li Z, Mouille G, Lea PJ, et al (2014) Assessing the metabolic impact of nitrogen availability using a compartmentalized maize leaf genome-scale model. Plant Physiol **166:** 1659–1674

Sims RE, Mabee W, Saddler JN, Taylor M (2010) An overview of second generation biofuel technologies. Bioresour Technol **101:** 1570–1580

Studer MH, DeMartini JD, Davis MF, Sykes RW, Davison B, Keller M, Tuskan GA, Wyman CE (2011) Lignin content in natural Populus variants affects sugar release. Proc Natl Acad Sci USA **108:** 6300–6305

Sullivan S, Ralet MC, Berger A, Diatloff E, Bischoff V, Gonneau M, Marion-Poll A, North HM (2011) CESA5 is required for the synthesis of cellulose with a role in structuring the adherent mucilage of Arabidopsis seeds. Plant Physiol **156:** 1725–1739

Tixier A, Cochard H, Badel E, Dusotoit-Coucaud A, Jansen S, Herbette S (2013) Arabidopsis thaliana as a model species for xylem hydraulics: does size matter? J Exp Bot **64:** 2295–2305

Tominaga-Wada R, Iwata M, Sugiyama J, Kotake T, Ishida T, Yokoyama R, Nishitani K, Okada K, Wada T (2009) The GLABRA2 homeodomain protein directly regulates CESA5 and XTH17 gene expression in Arabidopsis roots. Plant J **60:** 564–574

Turner S, Sieburth LE (2003) Vascular patterning. The Arabidopsis Book **2:** e0073, doi/10.1199/tab.0073

Urbanowicz BR, Peña MJ, Moniz HA, Moremen KW, York WS (2014) Two Arabidopsis proteins synthesize acetylated xylan in vitro. Plant J **80:** 197–206

Van Acker R, Vanholme R, Storme V, Mortimer JC, Dupree P, Boerjan W (2013) Lignin biosynthesis perturbations affect secondary cell wall composition and saccharification yield in Arabidopsis thaliana. Biotechnol Biofuels **6:** 46

Vissenberg K, Oyama M, Osato Y, Yokoyama R, Verbelen JP, Nishitani K (2005) Differential expression of AtXTH17, AtXTH18, AtXTH19 and AtXTH20 genes in Arabidopsis roots: physiological roles in specification in cell wall construction. Plant Cell Physiol **46:** 192–200

Xin Z, Browse J (1998) Eskimo1 mutants of Arabidopsis are constitutively freezing-tolerant. Proc Natl Acad Sci USA **95:** 7799–7804

Xiong G, Cheng K, Pauly M (2013) Xylan O-acetylation impacts xylem development and enzymatic recalcitrance as indicated by the Arabidopsis mutant tbl29. Mol Plant **6:** 1373–1375

Ye ZH, Freshour G, Hahn MG, Burk DH, Zhong R (2002) Vascular development in Arabidopsis. Int Rev Cytol **220:** 225–256

Yuan Y, Teng Q, Zhong R, Ye ZH (2013) The Arabidopsis DUF231 domain-containing protein ESK1 mediates 2-O- and 3-O-acetylation of xylosyl residues in xylan. Plant Cell Physiol **54:** 1186–1199